

Cite this: *Nanoscale*, 2015, 7, 8122

Synthesis-atomic structure-properties relationships in metallic nanoparticles by total scattering experiments and 3D computer simulations: case of Pt–Ru nanoalloy catalysts†

Binay Prasai,^a Yang Ren,^b Shiyao Shan,^c Yinguang Zhao,^c Hannah Cronk,^c Jin Luo,^c Chuan-Jian Zhong^c and Valeri Petkov*^a

An approach to determining the 3D atomic structure of metallic nanoparticles (NPs) in fine detail and using the unique knowledge obtained for rationalizing their synthesis and properties targeted for optimization is described and exemplified on Pt–Ru alloy NPs of importance to the development of devices for clean energy conversion such as fuel cells. In particular, Pt_xRu_{100-x} alloy NPs, where $x = 31, 49$ and 75 , are synthesized by wet chemistry and activated catalytically by a post-synthesis treatment involving heating under controlled N₂–H₂ atmosphere. So-activated NPs are evaluated as catalysts for gas-phase CO oxidation and ethanol electro-oxidation reactions taking place in fuel cells. Both as-synthesized and activated NPs are characterized structurally by total scattering experiments involving high-energy synchrotron X-ray diffraction coupled to atomic pair distribution functions (PDFs) analysis. 3D structure models both for as-synthesized and activated NPs are built by molecular dynamics simulations based on the archetypal for current theoretical modelling Sutton–Chen method. Models are refined against the experimental PDF data by reverse Monte Carlo simulations and analysed in terms of prime structural characteristics such as metal-to-metal bond lengths, bond angles and first coordination numbers for Pt and Ru atoms. Analysis indicates that, though of a similar type, the atomic structure of as-synthesized and respective activated NPs differ in several details of importance to NP catalytic properties. Structural characteristics of activated NPs and data for their catalytic activity are compared side by side and strong evidence found that electronic effects, indicated by significant changes in Pt–Pt and Ru–Ru metal bond lengths at NP surface, and practically unrecognized so far atomic ensemble effects, indicated by distinct stacking of atomic layers near NP surface and prevalence of particular configurations of Pt and Ru atoms in these layers, contribute to the observed enhancement of the catalytic activity of Pt_xRu_{100-x} alloy NPs at $x \sim 50$. Implications of so-established relationships between the atomic structure and catalytic activity of Pt–Ru alloy NPs on efforts aimed at improving further the latter by tuning-up the former are discussed and the usefulness of detailed NP structure studies to advancing science and technology of metallic NPs – exemplified.

Received 3rd February 2015,

Accepted 3rd April 2015

DOI: 10.1039/c5nr00800j

www.rsc.org/nanoscale

Introduction

With current science and technology moving rapidly into smaller scales, metallic nanoparticles (NPs) are synthesized in

increasing numbers and explored for various useful applications ranging from catalysis^{1–3} and photonics^{4,5} to magnetic storage media^{6–8} and drug delivery.^{9–11} Catalytic applications are of particular importance since, at present, virtually all transportation fuels and most chemicals are produced by technologies based on catalysis.¹² Among others, a few nanometre in size Noble metals-based alloy particles have shown a great promise as catalysts for several technologically important reactions because not only the particles have a large surface to volume ratio but also allow achieving higher catalytic activity and better selectivity by exploiting the synergy of metallic species alloyed. Advancing science and technology of metallic NPs, including metallic nanoalloy catalysts, however, face a

^aDepartment of Physics, Central Michigan University, Mt. Pleasant, Michigan 48858, USA. E-mail: petko1vg@cmich.edu

^bX-ray Science Division, Advanced Photon Source, Argonne National Laboratory, Argonne, Illinois 60439, USA

^cDepartment of Chemistry, State University of New York at Binghamton, New York 13902, USA

† Electronic supplementary information (ESI) available: XRD patterns, TEM and 3D structure modelling methodology. See DOI: 10.1039/c5nr00800j

major hurdle concerning transforming the current, largely trial-and-error route to synthesizing metallic NPs into synthesizing and optimizing metallic NPs for practical applications by rational design. This is not a trivial task since the outcome of synthesis and optimization of metallic NPs, typically done relevant by post-synthesis treatment, depend on a number of hard to assess kinetic and thermodynamic factors. Among others, an important step toward overcoming the hurdle would be the implementation and validation of an approach to determining the outcome of synthesis and optimization of metallic NPs at atomic level, that is the atomic-level structure of actual metallic NPs produced, and then using the unique knowledge obtained for rationalizing NP synthesis and properties targeted for optimization.

Indeed several experimental techniques such as coherent diffraction,¹³ high resolution Transmission Electron Microscopy (HR-TEM),¹⁴ Extended X-ray Absorption Fine Structure (EXAFS) spectroscopy,¹⁵ and others, have proven useful in structure studies of metallic NPs, including nanoalloy catalysts. However, due to their character, these techniques have not been able to determine the 3D atomic structure in fine detail but reveal some structural features of metallic NPs only. Recently total scattering coupled to atomic pair distribution functions (PDFs) analysis have emerged as a very efficient technique for structural characterization of materials confined to nanoscale dimensions, including metallic NPs.¹⁶ Here we augment the technique with 3D computer simulations and apply it to Pt–Ru nanoalloy catalysts. Among other families of metallic alloy NPs explored for catalytic applications, Pt–Ru one was chosen because of its importance for the development of currently highly pursued devices for clean energy conversion such as fuel cells, in particular for the family's remarkable ability to speed up gas-phase CO oxidation and ethanol electro-oxidation reactions taking place in fuel cells. The former entails the application of Pt–Ru alloy NPs as catalysts for the hydrogen oxidation reaction (HOR) taking place at the anode of Proton Exchange Membrane Fuel Cells (PEMFCs). The latter entails the application of Pt–Ru alloy NPs as catalysts in liquid fuel cells. Note, nanoalloy catalysts for HOR in PEMFCs are very much needed since, in the current state of technology, inexpensive hydrogen gas comes mostly from steam reforming of hydrocarbons. "Reformate" hydrogen, however, contains some impurities such as CO poisoning monometallic Pt NPs typically used as PEMFC anode catalysts leading to a severe degradation of PEMFCs performance. Supported Pt–Ru bulk and surface alloy NPs have emerged as a CO-tolerant and so very efficient PEMFC anode catalysts thus generating considerable research interest recently.^{17–21} Pt–Ru alloy NPs have also shown good promise as electro-catalysts for methanol oxidation in direct methanol fuel cells (DMFCs) wherein the oxidation of CO species resulted from methanol decomposition needs to be promoted.^{22–25} Here we pay particular attention to the electro-catalytic properties of Pt–Ru alloy NPs not in methanol but in direct ethanol fuel cells (DEFCs). Those are very attractive since ethanol not only has higher energy density (8.0 kW h kg⁻¹ vs. 6.1 kW h kg⁻¹)

than methanol but also is bio-renewable and not toxic. A key challenge to the commercial viability of DEFCs is the development of catalysts that can alleviate the formation of undesired by-products from ethanol decomposition such as acetic acid and acetaldehyde by effective cleavage of C–C bonds and accelerate the oxidation of CO species poisoning the reaction. Pt–Ru alloy NPs have shown very good promise in this regard as well.^{26,27} However, the numerous studies on Pt–Ru alloy NPs carried out so far have focused mostly on their catalytic properties and so provided limited knowledge about NP atomic structure. Here we concentrate on determining the atomic structure of Pt–Ru alloy NPs in fine detail, establishing the relationships between their atomic structure and catalytic properties, and demonstrating how these relationships can provide a feedback loop for streamlining synthesis and so optimizing performance of Pt–Ru alloy NPs in fuel cells related applications. For the purpose:

(i) Synthesized Pt_xRu_{100-x} alloy NPs ($x = 31, 49$ and 75) by wet chemistry and activated them catalytically by a controlled post-synthesis treatment involving heating in N₂–H₂ atmosphere.

(ii) Determined the morphology, *i.e.* size and shape, of both as-synthesized and post-synthesis treated Pt–Ru alloy NPs by TEM.

(iii) Determined the chemical pattern of Pt and Ru species across NPs by High-Angle Annular Dark-Field (HAADF) Scanning TEM (STEM) experiments.

(iv) Characterized structurally both as-synthesized and post-synthesis treated Pt–Ru NPs by total scattering experiments involving high-energy synchrotron X-ray diffraction (XRD) and atomic PDFs analysis.^{16,28–30}

(v) Built 3D structure models for both as-synthesized and post-synthesis treated NPs by Molecular Dynamics (MD) simulations based on the archetypal for current metal and alloy structure theory Sutton–Chen (SC) method.^{31,32} Simulations required developing SC potential for Ru since, contrary to the case of face-centered-cubic (fcc) metals such as Pt, SC potentials for hexagonal-close-packed (hcp) metals such as Ru are not readily available.

(vi) Refined MD models by reverse Monte Carlo (RMC) simulations guided by the experimental atomic PDFs.

(vii) Analysed RMC refined models in terms of structural characteristics important for catalysis such as NP phase state, distribution of first atomic neighbour distances, *i.e.* metal-to-metal bond lengths, first atomic coordination numbers and bond angles paying particular attention to Pt and Ru atoms at NP surface since it is the NP surface where catalytic reactions take place.

(viii) Measured the catalytic activity of post-synthesis treated, *i.e.* activated for catalytic applications, Pt–Ru alloy NPs for gas-phase oxidation of CO and electro-oxidation of ethanol.

(ix) Correlated data for catalytic activity with structural characteristics of respective NPs and established which of the latter are most likely to contribute to the observed enhancement of the former at $x \sim 50$.

(x) Based on so-established relationships between the atomic structure and catalytic activity of Pt–Ru alloy NPs suggested routes to improving further the latter by tuning up the former.

Experimental

Pt_xRu_{100-x} NPs ($x = 31, 49$ and 75) synthesis and post-synthesis treatment

Pt–Ru alloy NPs were synthesized by a protocol fully described in ref. 33. In brief, platinum(II) acetylacetonate and ruthenium(II) acetylacetonate were mixed in the desired molar ratio in octyl ether solution under N₂ atmosphere. Oleic acid and oleylamine were added to the solution as NP capping agents and 1,2-hexadecanediol – as a reducing agent. The solution was purged with N₂, heated to 220 °C and kept at that temperature for 30 min. After the solution cooled back to room temperature, the resulting Pt–Ru NPs were precipitated out by adding ethanol followed by centrifugation. Precipitated NPs were redispersed in hexane and mixed with fine carbon powder (XC-72) followed by sonication and overnight stirring. The resulting carbon supported Pt–Ru NPs, hereafter referred to as “as-synthesized”, were collected and dried under N₂ atmosphere. Then, in line with common practices, carbon supported Pt–Ru NPs were activated for catalytic applications. The activation involved a two-step thermal treatment under controlled gas atmosphere.³⁴ In particular, at first NPs were heated to 260 °C under N₂ atmosphere aiming at removing the organic molecules capping their surface. Next, NPs were further heated to 400 °C under 15 vol% H₂ atmosphere and kept at that temperature for 2 h. So post-synthesis treated NPs hereafter are referred to as “fully activated catalytically”. The loading of Pt–Ru NPs on the carbon support was determined by thermogravimetric analysis (TGA) performed on a Perkin-Elmer Pyris 1-TGA instrument, and found to be within 15–20% by weight.

Pt_xRu_{100-x} NPs ($x = 31, 49$ and 75) size, shape, chemical composition and chemical pattern determination

The size and shape of as-synthesized and fully activated Pt–Ru NPs were determined by TEM. For the measurements batches of NPs were diluted in hexane and drop cast onto carbon-coated copper grids followed by solvent evaporation in air at room temperature. The measurements were done on JEM-2200FS microscope operated at 200 kV. The microscope was fitted with an ultra-high-resolution (UHR) pole piece with a point resolution of 0.19 nm. Exemplary TEM and high-resolution (HR)-TEM images of as-synthesized and fully activated Pt_xRu_{100-x} alloy NPs ($x = 31, 49$ and 75) are shown in Fig. S1 and S2,† respectively. As can be seen in the figures (i) as-synthesized NPs are approximately 4.3(±0.6) nm in size and spherical in shape, (ii) fully activated NPs largely retain the spherical shape of as-synthesized ones and slightly increase in size to approximately 4.6(±0.7) nm and (iii) all NPs exhibit good overall crystallinity and, as usual for metallic NPs, some surface structural disorder.

The chemical composition of as-synthesized and fully activated Pt_xRu_{100-x} NPs ($x = 31, 49, 75$) was determined by inductively coupled plasma atomic emission spectroscopy (ICP-AES) carried out on a batch of samples for each x . Experiments were done on a Perkin Elmer 2000 DV ICP-OES instrument using a cross flow nebulizer with the following parameters: plasma 18.0 L Ar_(g) min⁻¹; auxiliary 0.3 L Ar_(g) min⁻¹; nebulizer 0.73 L Ar_(g) min⁻¹; power 1500 W; peristaltic pump rate 1.40 mL min⁻¹. Samples were dissolved in aqua regia, and then diluted to concentrations in the range of 1 to 50 ppm. Calibration curves were made from dissolved standards in the same acid matrix as the unknowns. Standards and the unknowns were analysed 10 times each resulting in <3% error in the reported chemical composition. Within the error limits no appreciable difference between the chemical composition of as-synthesized and respective fully activated Pt–Ru NPs was observed. Note, similar results, *i.e.* that a thermo-chemical activation of Noble metals-based NPs for catalytic applications conducted with due care does not necessarily induce significant changes in NP overall chemical composition, size and shape, have been reported by Dash *et al.*³⁵

The chemical pattern of fully activated Pt_xRu_{100-x} NPs ($x = 31, 49, 75$) was determined by High-Angle Annular Dark-Field (HAADF) Scanning TEM (STEM) experiments. Experiments were done on a JEOL JEM 2100F instrument equipped with a CEOS hexapole probe. The instrument was operated at 200 keV in STEM mode. The lens settings combined with the corrector tuning gave a spatial resolution of ~90 pm. Exemplary HAADF-STEM images are shown in Fig. S3.† Images indicate that fully activated Pt₄₉Ru₅₁ and Pt₇₅Ru₂₅ NPs are largely monophase alloys while Pt₃₁Ru₆₉ NPs are partially segregated alloys. Atomic PDFs analysis and 3D structure modelling described below confirmed the results of HAADF-STEM experiments.

Total scattering experiments

Carbon supported as-synthesized and respective fully activated Pt_xRu_{100-x} alloy NPs ($x = 31, 49$ and 75) were subjected to high-energy synchrotron X-ray diffraction (XRD) experiments at the 11-ID-C beamline of the Advanced Photon Source, Argonne. X-rays of energy 115 keV ($\lambda = 0.1080$ Å) were used. Diffraction data was collected on a large area detector up to wave vectors of 25 Å⁻¹ allowing resolving structural features of NPs in fine detail. The experimental set-up was calibrated with high-purity powder Si standard. During the measurements samples were sealed in thin-walled glass capillaries. An empty glass capillary and carbon powder alone were measured separately. Experimental synchrotron high-energy XRD patterns corrected for sample absorption, empty glass capillary, carbon support and other background-type (air *etc.*) scattering are shown in Fig. S4.† Patterns exhibit a few broad, strongly overlapping peaks at low diffraction (Bragg) angles and almost no distinct peaks at high diffraction angles, *i.e.* are rather diffuse in nature. This rendered the well-established, sharp Bragg peaks-based procedures for determining the atomic-scale structure of bulk metals and alloys inapplicable to Pt–Ru alloy NPs studied here. Therefore, the diffuse XRD patterns were reduced

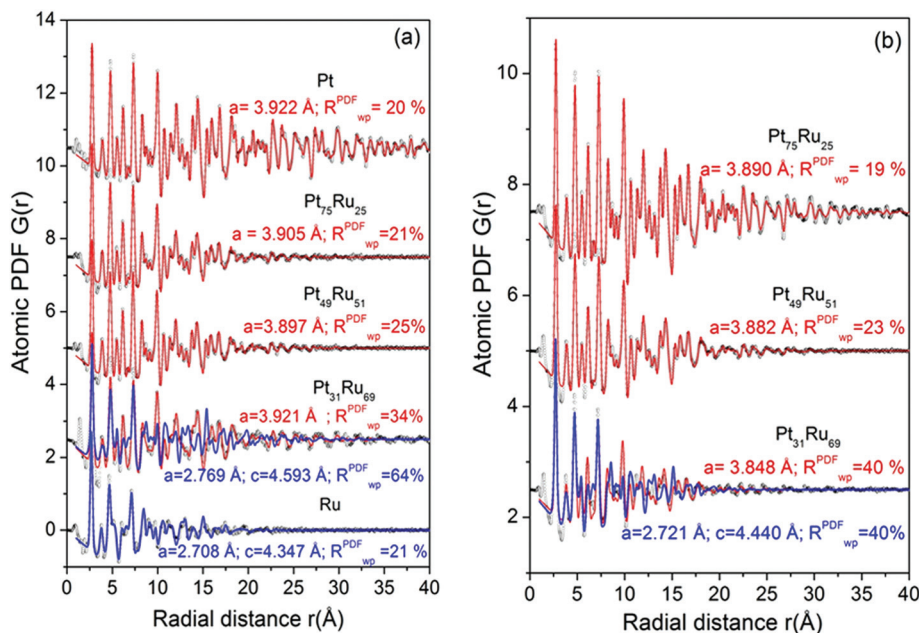


Fig. 1 Experimental (symbols) and model (lines) PDFs for as-synthesized (a) and post-synthesis treated (b) $\text{Pt}_x\text{Ru}_{100-x}$ alloy NPs ($x = 31, 49$ and 75). Model PDFs based on a hcp-type crystal structure are given in blue while those based on a fcc-type crystal structure – in red. Values of “hcp- and fcc-lattice parameters”, derived by adjusting structure models against the respective experimental PDFs, are given by each data set. Model’s quality indicators, $R_{\text{wp}}^{\text{PDF}}$, explained in ESI,† are shown by each data set in color pertaining to the respective structure model. Experimental and model atomic PDFs for ~ 7 nm in size pure Pt particles and ~ 3.5 nm in size pure Ru particles, obtained by independent studies, are also shown in (a) to facilitate differentiating between the structural features of hcp(Ru) and fcc(Pt)-type models.

to the so-called atomic PDFs $G(r)$ following well-established procedures.³⁶ The approach is advantageous^{28–30} since, contrary to the respective diffuse XRD patterns, atomic PDFs show several distinct peaks allowing convenient testing and refinement of atomic-structure models for NPs. Atomic PDFs $G(r)$ derived from the XRD patterns of Fig. S4† are shown in Fig. 1. Note, XRD patterns of Fig. S4† and so their Fourier counterparts, the atomic PDFs of Fig. 1, reflect ensemble averaged structural features of all Pt–Ru NPs sampled by the X-ray beam in a way traditional powder XRD patterns reflect ensemble averaged structural features of all polycrystallites sampled by the X-ray beam in those experiments. Using NP ensemble averaged structural features to understand and explain NP ensemble averaged properties (*e.g.* catalytic, magnetic, optical *etc.*) puts NP atomic structure–properties exploration on the same footing. Also, note, by definition, atomic PDFs $G(r)$ peak at distances separating all pairs of atoms within the material studied. Accordingly, the experimental PDFs of Fig. 1 peak at distances separating Pt–Pt, Pt–Ru and Ru–Ru pairs of atoms, immediate and all farther neighbours, within Pt–Ru NPs studied here. Since atoms at/close to opposite sides of NPs are separated most, the atomic PDFs of Fig. 1 may show distinct peaks up to distances close to the average size (diameter) of the respective NPs. As can be seen in Fig. 1, however, peaks in the experimental PDFs decay to zero at distances (~ 3.5 nm) shorter than the physical size of respective NPs, which is ~ 4.5 nm as determined by TEM. The observed fast decay of

the experimental PDFs indicates that surface atoms in Pt–Ru alloy NPs suffer non-negligible positional disorder. Such is common to metallic NPs due to NP finite size and surface relaxation effects.^{13–15,28–30}

Catalytic activity measurement

The catalytic activity of fully activated $\text{Pt}_x\text{Ru}_{100-x}$ alloy NPs ($x = 31, 49$ and 75) for gas-phase oxidation of CO was measured under CO (0.5 vol% balanced by N_2) + O_2 (10 vol% balanced by N_2) atmosphere using a custom-built system including a temperature-controlled reactor, a gas flow/mixing/injection controller, an on-line gas chromatograph (Shimadzu GC 8A) equipped with 5A molecular sieve, Porapak Q packed columns and a thermal conductivity detector. Carbon supported NPs were loaded in a quartz microreactor tubing with an inner diameter of 4 mm and the tubing was wrapped with quartz wool. The feeding gas (0.5 vol% CO + 10 vol% O_2 balanced by N_2) was injected continuously through the fixed NPs’ bed (~ 6 mm in length) at a flow rate of 20 mL min^{-1} . The residence time was about 0.2 seconds. Gas hourly space velocity (GHSV) in the system was about $16\,000 \text{ h}^{-1}$. The amount of highly reactive and toxic CO oxidized to largely inert and harmless CO_2 was determined by analysing the composition of tail gas effusing from the quartz microreactor using the on-line (Shimadzu GC 8A) gas chromatograph.

The catalytic activity of fully activated $\text{Pt}_x\text{Ru}_{100-x}$ alloy NPs ($x = 31, 49$ and 75) for electro-oxidation of ethanol was

measured following a widely adopted procedure described in ref. 37. In brief, for each x , a suspension of the carbon supported NPs was prepared by dissolving 10 mg of NPs in 10 ml of water containing 5% vol. of Nafion polymer. The suspension was ultrasonicated for 10 min until it turned into a dark ink. 10 μ L of the ink were uniformly distributed over the surface of a polished, glassy carbon disk with a surface area of 0.196 cm². The disc, as coated with a thin film of the ink, was dried overnight at room temperature, inserted into an electrochemical cell and used as cell's working electrode. The cell included two more electrodes, one known as a reference (Ag/AgCl, saturated KCl) electrode and the other – as a counter (Pt) electrode. Those were positioned in separate compartment of the cell. Electrolyte was made by dissolving KOH pellets (optimal grade) in Milli-Q water as to achieve a concentration of 0.5 M KOH. Ethanol was added until its concentration in the electrolyte also reached 0.5 M level. The electrolyte was deaerated with high purity N₂ before conducting cyclic voltammetry (CV) sweeps at room temperature. Current generated by the cell was measured while the potential of the working electrode was varied between -0.9 and $+0.5$ V. Note, in CV measurements, typically, “forward current” pertains to the current generated while the potential of working electrode goes from negative (-0.9 V) to positive ($+0.5$ V). Accordingly, “backward current” pertains to the current generated while the potential of working electrode goes from positive ($+0.5$ V) to negative (-0.9 V). Data for the electrocatalytic activity of fully activated Pt–Ru alloy NPs presented here reflect the peak values of “forward” current as normalized against the amount of Pt loaded in the catalyst on the working electrode.

Results and discussion

When alloyed in bulk, fcc Pt and hcp Ru straddle a stability limit in the binary phase diagram even when annealed at temperature above 1000 °C.³⁸ In particular, solids containing more than 50 at% of Pt tend to crystallize in a fcc-type structure. On the other hand, solids containing less than 20 at% of Pt tend to crystallize in a hcp-type structure. Solids containing from 20 to 50 at% Pt tend to segregate into coexisting hcp(Ru-rich) and fcc(Pt-rich) type phases. Pt _{x} Ru_{100- x} alloy NPs ($x = 31, 49$ and 75) studied here were synthesized and post-synthesis treated at temperature much lower than 1000 °C. Therefore, the type of their atomic-scale structure could not be inferred for sure from that of Pt–Ru solids of similar chemical composition. Besides, studies have shown that metals and alloys confined to nanoscale dimensions do not necessarily adopt the structure type of their bulk counterparts.^{39–41} The structure type of Pt–Ru alloy NPs studied here was determined by approaching the respective experimental atomic PDFs with purely empirical models constrained to the fcc- and hcp-type perfectly 3D periodic, infinite lattices used to describe the crystal structure of bulk Pt and Ru, respectively. The δ -function like peaks in the atomic PDFs derived from the model lattices were broadened by convolution with gaussian functions as to

mimic the dynamic (*i.e.* thermal) and static structural disorder usually present in metallic NPs. At the same time model PDFs were multiplied by an artificial, rapidly decaying with real space distances function as to mimic the finite size (~ 4.5 nm) of Pt–Ru NPs. Finally, the unit cell parameters of model fcc- and hcp-lattices were refined so that the model-derived atomic PDFs approached the experimental ones as close as possible. Here it may be noted that “lattice parameters” of metallic NPs are not as well defined as a physical quantity as those for their bulk counterparts. The reason is that “lattice parameters” imply the presence of perfectly 3D periodic, infinite lattices while metallic NPs are finite and not necessarily perfectly 3D periodic at atomic level. Nevertheless, total scattering/PDF data-derived “lattice parameters” of metallic NPs are useful merely because they reflect the set of interatomic distances, including metal-to-metal bond lengths, characteristic for the actual NPs under study and, hence, may be used as a trustworthy “global indicator” of those distances. Modeling was done with the help of program PDFgui.⁴² Results from the modeling are shown in Fig. 1.

As can be seen in the figure, models featuring a fcc-type crystal structure reproduce very well ($R_{\text{wp}}^{\text{PDF}} \sim 19\text{--}21\%$) the experimental PDFs for as-synthesized and respective fully activated Pt₇₅Ru₂₅ NPs indicating that atoms in these NPs are fcc-type ordered. Models featuring a fcc-type crystal structure reproduce the experimental PDFs for as-synthesized and respective fully activated Pt₄₉Ru₅₁ NPs at an acceptable level ($R_{\text{wp}}^{\text{PDF}} \sim 23\text{--}25\%$) indicating that atoms in these NPs are largely but not entirely fcc-like ordered. Some features in the experimental PDFs for as-synthesized and respective fully activated Pt₃₁Ru₆₉ NPs are reproduced well by a fcc-type model while others – by a hcp-type one. However, neither a fcc- ($R_{\text{wp}}^{\text{PDF}} \sim 34\text{--}40\%$) nor a hcp-type ($R_{\text{wp}}^{\text{PDF}} \sim 40\text{--}46\%$) model alone reproduce the experimental PDF data well indicating that atoms in Pt₃₁Ru₆₉ NPs studied here are, very likely, segregated into domains each with a distinct fcc- or hcp-type structure.

Inspection of data in Fig. 1 also reveals that the characteristic interatomic distances both in as-synthesized and fully activated Pt _{x} Ru_{100- x} alloy NPs ($x = 31, 49$ and 75), as reflected by the respective PDF-derived “lattice parameters”, are significantly different from those in bulk fcc Pt ($a = 3.924$ Å) and hcp Ru ($a = 2.704$ Å and $c = 4.281$ Å). Furthermore, it reveals that the post-synthesis treatment of NPs (i) diminishes atomic positional disorder in Pt₇₅Ru₂₅ NPs (see the difference in the sharpness of the peaks in the respective PDFs), (ii) does not affect atomic positional disorder in Pt₄₉Ru₅₁ NPs substantially (see the similar sharpness of the peaks in the respective PDFs) and (iii) increases atomic positional disorder in Pt₃₁Ru₆₉ NPs (see the faster decay of the atomic PDF for post-synthesis treated sample to zero). Indeed (i) to (iii) are easier to acknowledge by inspecting data in Fig. 4 introduced later on. In general, the empirical modeling indicated that Pt _{x} Ru_{100- x} alloy NPs ($x = 31, 49$ and 75) studied here adopt a fcc- and/or hcp-like atomic structure but exhibit a unique degree of atomic positional disorder and/or partial segregation for any given x .

Accounting for the findings of simplistic empirical modeling realistic 3D models both for as-synthesized and post-synthesis treated Pt–Ru alloy NPs were built by MD simulations based on the archetypal for current metal and alloy atomic structure theory Sutton–Chen (SC) method. Among other theoretical methods currently in use, SC one was chosen because of its simplicity and proven success.^{43,44} Method's basics are given as ESI.† SC parameters for Pt species adopting a fcc-type structure in bulk were taken from literature sources.^{31,32} Parameters are listed in Table S1.† SC parameters for Ru species adopting a hcp-type structure in bulk were derived by a well-established procedure described in ESI.† Parameters are listed in Table S2.† MD models featured NPs with the chemical composition, chemical pattern (see Fig. S3†), size (~ 4.5 nm) and shape (spherical; see Fig. S1 and S2†) of actual Pt–Ru alloy NPs studied here. Details of MD simulations are given as ESI.† Resulted 3D models are shown in Fig. S5.† Atomic PDFs derived from the models are compared with the respective experimental PDFs in Fig. 2.

As can be seen in Fig. 2 MD built structure models produce atomic PDFs that capture the essence of experimental ones but fail in reproducing them in fine detail. In particular, MD models fail in reproducing the position, broadening and intensity of several peaks in the experimental PDFs, *i.e.* the radii, degree of atomic positional disorder and atomic population of several coordination spheres in Pt–Ru alloy NPs. The inability of MD models to reproduce accurately the radii of atomic coordination spheres in $\text{Pt}_x\text{Ru}_{100-x}$ alloy NPs ($x = 31, 49$ and 75) may be expected since SC method^{31,32,45} employed by MD is, like most theoretical methods currently in use, validated

against experimental data for the lattice parameters of respective solids (see Tables S1 and S2†). Results of empirical modeling carried out here, however, showed clearly that NP “lattice parameters”, *i.e.* the characteristic interatomic distances in Pt–Ru alloy NPs, are different from these of the respective solids. Indeed this is a rather common observation since interatomic distances in metallic NPs can get “compressed” or “stretched out” considerably and non uniformly as a result of the inherently increased surface tension of NPs¹³ and/or NP surface environment effects such as, for example, exposure to reactive (*e.g.* H_2) gases.⁴⁶ Such an effect is atypical for the respective solids. Besides, charge transfer and optimization of atomic-level stresses in metallic alloy NPs can result in a considerable change in the radii/size of metallic species involved which, again, may not be the case with the respective solids.^{16,47} The inability of MD models to reproduce accurately the degree of local structural disorder in $\text{Pt}_x\text{Ru}_{100-x}$ alloy NPs ($x = 31, 49$ and 75), in particular its inherent enhancement in coordination spheres involving atoms close to/at the extended NP surface, may also be expected. It is due to the fact that MD treats all atoms in structure models alike whereas atoms inside and at the surface of real-world metallic NPs are not necessarily alike in respect to their immediate atomic neighborhood, and others. The inability of MD models to reproduce accurately the distribution of Pt and Ru atoms across NPs is not a big surprise either. The reason is that, typically, MD models feature atomic configurations quenched from some high temperature initial state while Pt–Ru alloy NPs studied here are synthesized in solution kept at room temperature and only then subjected to a treatment at elevated but not very high temperature. Nevertheless, as discussed in ref. 16, MD simulations are

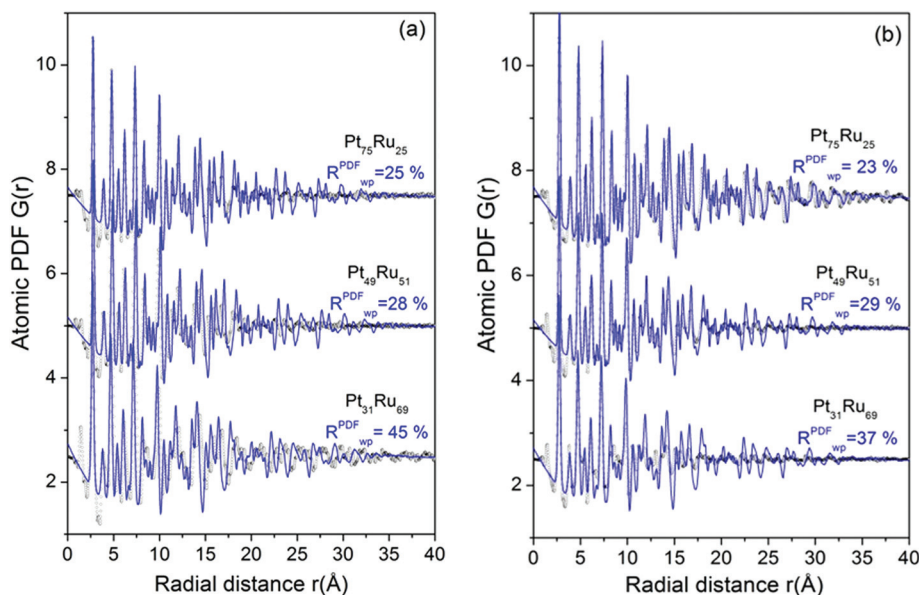


Fig. 2 Experimental (symbols) and model (lines in blue) PDFs for as-synthesized (a) and post-synthesis treated (b) $\text{Pt}_x\text{Ru}_{100-x}$ alloy NPs ($x = 31, 49$ and 75). Model PDFs are derived from 3D atomic configurations (see Fig. S5†) generated by MD simulations based on SC method as described in the text. Model's quality indicators, R_{wp}^{PDF} , explained in ESI,† are shown by each data set.

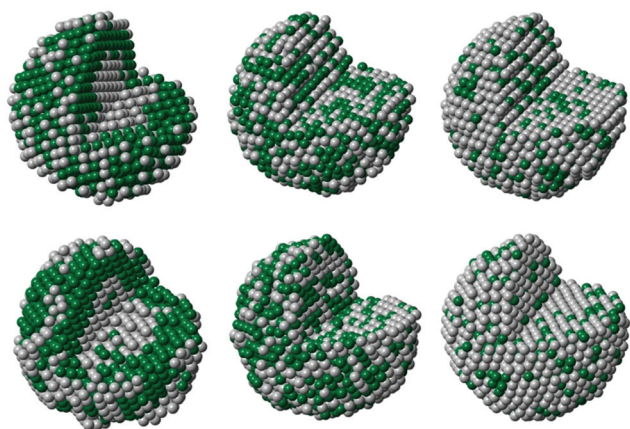


Fig. 3 RMC refined 3D structure models for as-synthesized (first row) and post-synthesis treated (second row) $\text{Pt}_x\text{Ru}_{100-x}$ alloy NPs ($x = 31$, left column); ($x = 49$, middle column) and ($x = 75$; right column). Models include approximately 3500 Pt and Ru atoms in due proportions. Ru atoms are in green and Pt – in gray. Note while Pt and Ru atoms both in as-synthesized and post-synthesis treated $\text{Pt}_{49}\text{Ru}_{51}$ and $\text{Pt}_{75}\text{Ru}_{25}$ NPs are well mixed together those in $\text{Pt}_{31}\text{Ru}_{69}$ NPs segregate (partially) into intertwined Pt-rich and Ru-rich domains. Domains in as-synthesized NPs seem to evolve somewhat when NPs are subjected to a post-synthesis treatment. The evolution is toward an “onion-like” chemical pattern wherein the “onion” core and surface get enriched in Pt atoms while the intermediate section of “onion” – in Ru atoms.

useful in providing plausible structure models for metallic NPs that can be refined further, when necessary.

To account for the combined effects of NP finite size, inherent and/or post-synthesis treatment induced NP “compression/stretching out”, likely optimization of atomic-level

stresses and charge transfer taking place upon alloying of Pt and Ru species at the nanoscale, MD models were refined further by RMC simulations. In the simulations positions of atoms in MD models of Fig. S5† were adjusted, including switching the positions of nearby Pt and Ru atoms, as that the difference between RMC model derived and respective experimental PDF data is reduced as much as possible. At the same time model’s energy was minimized, *i.e.* model’s stability maximized, to the fullest possible extent using reliable pairwise (Lennard-Jones type) potentials. More details of RMC simulations are given as ESI.† RMC refined models for $\text{Pt}_x\text{Ru}_{100-x}$ alloy NPs ($x = 31$, 49 and 75) are shown in Fig. 3. Atomic PDFs derived from the models are compared with the respective experimental PDFs in Fig. 4.

As can be seen in Fig. 4 atomic PDFs derived from RMC refined 3D structure models for Pt–Ru alloy NPs reproduce respective experimental atomic PDFs in very good detail (see the reported $R_{\text{wp}}^{\text{PDF}}$ factors), including the region of longer interatomic distances/higher r -values which, as discussed above, is sensitive to structural features of NP surface. Precise accounting for the latter is important for catalysis since it is the NP surface where catalytic reactions take place.

With 3D models of realistic size, shape, chemical composition, chemical species ordering pattern, type of atomic ordering and atomic coordination spheres, including coordination radii and numbers, tuned up against relevant experimental PDF data at hand all important structural characteristics of actual metallic NPs studied can be derived. Characteristics can be used for (i) revealing the outcome of particular synthesis and post-synthesis treatment protocol employed, (ii) considering NP properties of interest on a sound structural basis and (iii) establishing NP atomic structure–properties relationships.

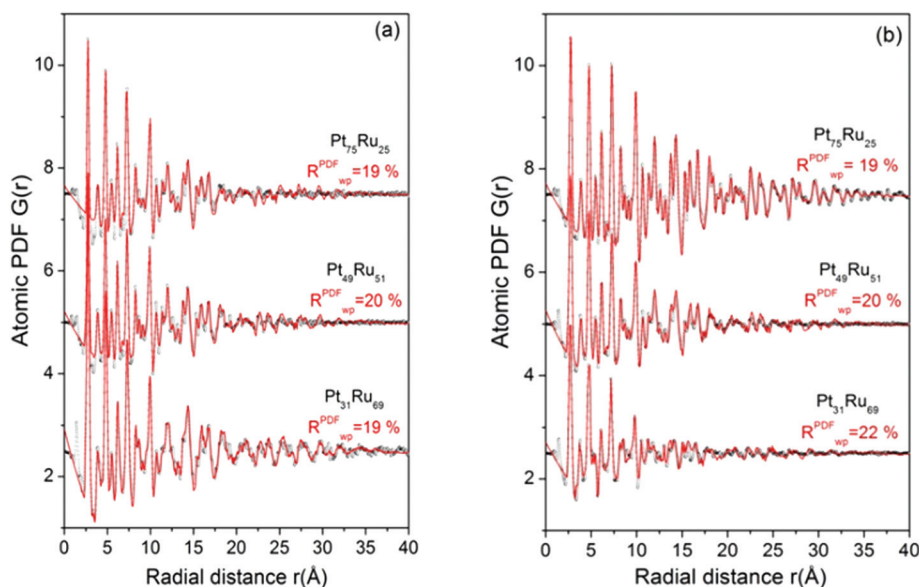


Fig. 4 Experimental (symbols) and model (lines in blue) PDFs for as-synthesized (a) and post-synthesis treated (b) $\text{Pt}_x\text{Ru}_{100-x}$ alloy NPs ($x = 31$, 49 and 75). Model PDFs are based on RMC refined atomic configurations shown in Fig. 3. Model’s quality indicators, $R_{\text{wp}}^{\text{PDF}}$, explained in ESI,† are shown by each data set.

Here we concentrate on structural characteristics relevant to catalytic properties of metallic NPs^{48–62} such as metal-to-metal bond lengths, bond angles and coordination numbers (CNs) paying particular attention to metallic species at NP surface. Note, bond angles are very sensitive to the type of local atomic ordering while metal-to-metal bond lengths and coordination numbers – to the strength of interactions between metallic species and how they configure in space, respectively. Metal-to-metal bond lengths inside and at the surface of as-synthesized and post-synthesis treated Pt–Ru alloy NPs, as derived from the respective RMC refined models, are presented in Tables S5 and S6,† respectively. First CNs inside and at the surface of NPs, as derived from the same models, are presented in Tables S7 and S8,† respectively. Distribution of Ru–Ru–Ru and Pt–Pt–Pt bond angles across as-synthesized and post-synthesis treated Pt–Ru alloy NPs are shown in Fig. S6 and S7,† respectively. Distribution of bond angles between all metallic species at the surface of post-synthesis treated NPs are shown in Fig. S8.† Data in Fig. S6–S8† also are derived from the models shown in Fig. 3, second row. Note, Pt–Pt–Pt and Ru–Ru–Ru bond angle distributions shown in Fig. S6 and S7† involve the immediate Pt neighbors of each Pt and the immediate Ru neighbors of each Ru species, respectively, across Pt–Ru alloy NPs., *i.e.* are sensitive to the type of metallic species involved. On the other hand, distributions of bond angles shown in Fig. S8† disregard the type of metallic species involved, *i.e.* are sensitive to the way metallic species pack altogether. Furthermore, they involve atoms forming the top three layers alone in post-synthesis treated Pt–Ru alloy NPs. Note, for fcc/hcp-type metallic particles ~4.5 nm in size the top three layers include ~35% of all atoms within the NPs. Being a volume sensitive technique total scattering coupled to atomic PDFs analysis is fully capable of revealing details in the atomic ordering in such large segments of NPs studied.

Data in Tables S7 and S8† indicate that the synthesis and post-synthesis treatment protocol employed here yield Pt_xRu_{100–x} NPs ($x = 31, 49$ and 75) wherein Pt and Ru atoms are packed closely both inside NPs (first CNs ~11.7) and at NPs surface (first CNs ~7.3). Data in Fig. S6 and S7† indicate that, locally, Pt atoms alone both in as-synthesized and post-synthesis treated Pt–Ru NPs are packed in a fcc-type manner maintaining the type of atomic ordering in bulk Pt. Ru atoms alone in as-synthesized and post-synthesis treated Ru-poor, *i.e.* Pt₇₅Ru₂₅ NPs also are packed in a fcc-type manner evidently adopting the type of packing of majority Pt atoms. On the other hand, Ru atoms alone in as-synthesized and post-synthesis treated Ru-rich, *i.e.* Pt₃₁Ru₆₉ NPs, and, to a certain extent, in Pt₄₉Ru₅₁ NPs appear packed in a hcp-type manner largely maintaining the type of atomic ordering in bulk Ru. Results are fully in line with the empirical modeling described above indicating that as-synthesized and post-synthesis treated Pt₇₅Ru₂₅ NPs clearly exhibit a fcc-type structure while as-synthesized and post-synthesis treated Pt₃₁Ru₆₉ NPs are partially segregated into domains each with a distinct fcc- or hcp-type structure. According the more sophisticated MD and RMC modeling these domains are rich in Pt and Ru species, respectively. Obviously,

both the close packed, metallic nature and the fcc and/or hcp-type ordering, of Pt and Ru species in Pt_xRu_{100–x} NPs ($x = 31, 49$ and 75) do not change significantly upon NP activation for catalytic applications by a thermo-chemical treatment of the type employed here. However, as data in Tables S5 and S6† indicate, finer details in NP atomic structure, such as first atomic neighbor distances, *i.e.* metal-to-metal bond lengths, change. In particular, Pt–Pt and Ru–Ru metal bond lengths in as-synthesized Pt_xRu_{100–x} NPs appear practically indistinguishable from those in bulk Pt (2.77 Å) and bulk Ru (2.67 Å), respectively. By contrast, metal-to-metal bond lengths in post-synthesis treated NPs largely appear shorter than those in as-synthesized NPs and respective solids indicating increased interactions between Pt and Ru metallic species. Moreover, the post-synthesis treatment induced shortening of metal-to-metal bond lengths appears irregular in a sense that (i) it does not evolve linearly with NP bimetallic composition and (ii) is more pronounced for atoms at NP surface. The post-synthesis treatment is also seen to change the way Pt and Ru species arrange with respect to each other as manifested by the significant differences between Pt–Pt, Pt–Ru and Ru–Ru first CNs in as-synthesized (Table S7†) and respective fully activated Pt–Ru NPs (Table S8†). The change is particularly prominent with Pt₃₁Ru₆₉ NPs wherein a large number of surface Ru atoms seem to have diffused into NP interior (surface Ru–Ru CN drops from 5.7 to 5.2) and a corresponding number of sub-surface Pt atoms moved toward NP surface (surface Pt–Pt CN increase from 1.9 to 4.2) resulting in a sharpening of the onion-like chemical pattern of the NPs, as exemplified in Fig. 3 (second row, left) and S8.† Other studies^{48,49} on Pt–Ru alloy NPs of low Pt content have also indicated a tendency of Pt species to segregate at NP surface and explained it with the fact that the surface energy of Pt (2.7 J m^{–2}) is lower than that of Ru (3.4 J m^{–2}). The fact that not all but only a fraction of Pt atoms segregates at NP surface and the rest cluster at NP center may be considered a manifestation of the so-called NP core–shell inversion effect. As shown in prior work^{63,64} different metallic species in binary alloy NPs may swap positions when the degree of atomic positional disorder and strain, due to metal bond lengths mismatch, reach a critical value. Often, a balance between the tendency of one of the two types of metallic species (*i.e.* Pt) in binary alloy NPs to segregate at NP surface and the NP (Ru)core–(Pt)shell inversion effect is reached by formation of an “onion-like” chemical pattern of the type shown in Fig. 3 (second row, left).⁶⁵

First neighbor Pt–Pt and Ru–Ru distances, *i.e.* metal-to-metal bond lengths, and first Pt–Pt and Pt–Ru CNs for Pt and Ru atoms at the surface of fully activated for catalytic applications Pt_xRu_{100–x} alloy NPs ($x = 31, 49$ and 75), as derived from their 3D structure models of Fig. 3 (second row), are shown in Fig. 5. Experimental data for the catalytic activity of same NPs for gas-phase oxidation of CO and electro-oxidation of ethanol, obtained as described in the Experimental section, are also shown in the figure. Inspection of so-summarized NP atomic structure *vs.* NP property data indicates that the catalytic activity of Pt–Ru alloy NPs studied here peaks when

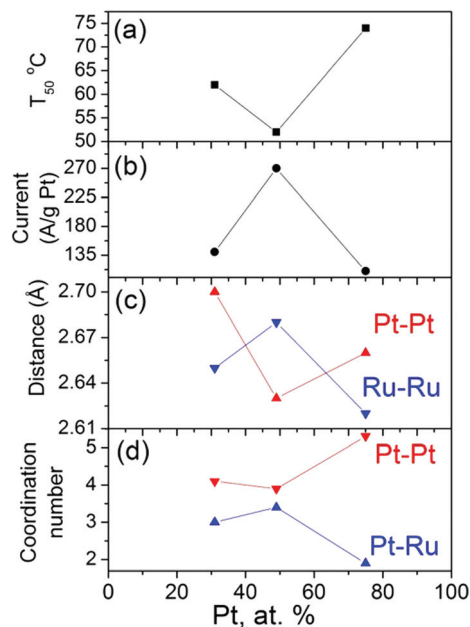


Fig. 5 (a) Catalytic activity of post-synthesis treated $\text{Pt}_x\text{Ru}_{100-x}$ alloy NPs ($x = 31, 49$ and 75) for gas-phase oxidation of CO given in terms of the temperature T_{50} at which 50% conversion of CO is achieved. Note the lower T_{50} the better the catalytic activity; (b) catalytic activity of post-synthesis treated $\text{Pt}_x\text{Ru}_{100-x}$ alloy NPs ($x = 31, 49$ and 75) for electro-oxidation of ethanol given in terms of peak current generated as a result of the reaction; (c) Pt–Pt and Ru–Ru bond lengths at the surface of post-synthesis treated $\text{Pt}_x\text{Ru}_{100-x}$ alloy NPs ($x = 31, 49$ and 75) and (d) first neighbor Pt–Pt and Pt–Ru CNs at the surface of same NPs. Note data in (a) and (b) are obtained as described in the Experimental section. Data in (c) and (d) are derived from RMC refined structure models shown in Fig. 3 (second row).

(i) Pt–Pt and Ru–Ru bond lengths at NP surface are, respectively, shortened and elongated most and (ii) surface Pt–Pt and Pt–Ru first CNs are nearly identical. To comprehend the observed NP atomic structure-catalytic activity relationships we reasoned them within the framework of three most frequently evoked explanations for the higher catalytic activity of metallic alloy NPs as compared to that of respective monometallic NPs. Those explanations argue that (i) different metallic species at the surface of alloy NPs do not interact but act cooperatively as to promote particular steps of chemical reactions, (ii) different metallic species at the surface of alloy NPs interact by exchanging charge and/or adjusting size both affecting their electronic structure in a way favorable for chemical reactions and (iii) different metallic species at NP surface assemble in particular configurations providing active catalytic sites.^{50–52} In the case of Pt–Ru alloy NPs explanation (i) has been put forward in terms of the so-called bi-functional mechanism^{53,54} envisioning formation of surface Ru-hydrate species easing CO oxidation on nearby surface Pt atoms. The mechanism, however, has been found incapable of explaining the improved catalytic activity of Pt–Ru NPs wherein Pt atoms completely cover NP surface thus screening all Ru atoms from chemical species adsorbed at that surface.^{17,20,21} On the other hand,

explanation (ii) has found strong support in numerous experimental and theoretical studies on Pt–Ru alloy NPs indicating the presence of charge transfer between Pt and Ru species^{55–59} accompanied by a considerable shortening of Pt–Pt and elongation of Ru–Ru metal bond lengths.^{50,52,60–62} According Pauling's theory of chemical bonds^{66,67} some charge transfer between Pt and Ru species may be expected due to their somewhat different electronegativity that is 2.3 and 2.2, respectively. Change in Pt–Pt and Ru–Ru bond lengths may also be expected since in order for the atomic-level stresses in Pt–Ru alloy NPs to be optimized the larger in size Pt species (2.77 Å) should “shrink” and the smaller in size Ru species (2.67 Å) – “expand” as that the ratio of their size/radii becomes as close to one as possible.^{67,68} Changes in metal-to-metal bond length, strength and the electronic structure of respective metal species are known to be largely interrelated^{66,67} and so difficult to take apart. Nevertheless, it has been shown that metal-to-metal bond length changes of the type shown in Fig. 5c would induce a strong downshift of the d electron states of surface Pt atoms in $\text{Pt}_x\text{Ru}_{100-x}$ alloy NPs at $x \sim 50$. This would modify the energies of bonding of chemical species to surface Pt atoms and so the activation barriers of critical steps of chemical reactions, such as gas-phase oxidation of CO and electro-oxidation of ethanol, in a way enhancing the catalytic activity of $\text{Pt}_x\text{Ru}_{100-x}$ alloy NPs for $x \sim 50$.^{50,52,60–62} Indeed this is exactly what data in Fig. 5(a and b) show. Explanation (iii) has been contemplated in several studies on Pt–Ru alloy NPs^{26,50,58,69,70} but not recognized explicitly so far. Data in Fig. 5 provides strong evidence that not only electronic (ii) but also atomic ensemble (iii) effects, signified by the prevalence of atomic configurations where both Pt and Ru metal species have pretty much the same number of unlike first neighbors (Pt–Pt and Pt–Ru first CNs of 3.8 and 3.5, and Ru–Pt and Ru–Ru CNs of 3.5 and 3.8, respectively, see Table S8†), contribute to the enhanced catalytic activity of $\text{Pt}_x\text{Ru}_{100-x}$ alloy NPs for $x \sim 50$. The fact (see Fig. S8†) that near surface atomic layers in $\text{Pt}_x\text{Ru}_{100-x}$ alloy NPs are largely stacked in a hcp-like manner for $x \sim 50$ while those in $\text{Pt}_x\text{Ru}_{100-x}$ alloy NPs of lower ($x = 31$) and higher ($x = 75$) Pt content appear fcc-like stacked is another indication that atomic ensemble effects, this time signified by distinct stacking of atomic layers near NP surface, contribute to the enhancement of catalytic activity of $\text{Pt}_x\text{Ru}_{100-x}$ alloy NPs for $x \sim 50$. Note, electronic and atomic ensemble effects described above do not contradict but complement each other since it is when both metallic species at the surface of binary alloy NPs are closely packed altogether and have pretty much the same number of unlike first neighbors to interact with the likelihood of (i) charge transfer between the species and/or (ii) sizable adjusting of species' size is maximized. Also, note, our findings do not dismiss the “bi-functional” mechanism (i). Rather, they highlight that it is the optimal combination of downshift of d electron states of surface Pt atoms, surface Pt–Pt and Ru–Ru metal bond lengths, surface Pt–Pt and Pt–Ru CNs and stacking of near surface atomic layers in $\text{Pt}_{100-x}\text{Ru}_x$ alloy NPs with $x \sim 50$ what enables an efficient cross-reactivity of reaction

intermediates on the different catalytic sites, such as transfer of activated or intermediate CO-species to sites favoring a reaction with activated O-species, and/or refreshing the catalytic sites, resulting in reducing the propensity of positioning.

With the relationships between atomic structure and catalytic activity of Pt–Ru alloy NPs established and understood well useful clues to improving further the latter by tuning up the former can be contemplated. For example, it may be conjectured that a synthesis and post-synthesis protocol aimed at (i) stacking atomic layers near NP surface in a hcp-type manner, (ii) densely populating those layers with Pt and Ru atoms so that each of them would have a close to the maximum possible number of unlike first neighbours and (iii) strengthening the interactions between Pt and Ru species near NP surface as that Pt–Pt and Ru–Ru metal bond lengths “contract” and “expand”, respectively, may be a rather successful route to producing Pt–Ru alloy NPs with improved catalytic activity for gas-phase oxidation of CO and electro-oxidation of ethanol. Achieving each of (i), (ii) and (iii) is important since the catalytic activity, configuring of surface metallic species, surface metal-to-metal bond lengths and strength, *i.e.* electronic structure of surface metallic species, are intimately coupled.^{50,52,62,71–74} Also, it may be conjectured that such a route may lead to catalysts with improved durability since studies have shown that well alloyed Pt–Ru NPs are more stable in catalytic reactions than partially segregated ones.^{75,76} Furthermore, the route would facilitate adding a third metallic species, such as Mo, W or Sn, to the mix of Ru and Pt species as to stabilize certain quasi-ternary nanoalloys with excellent catalytic properties for electro-oxidation of ethanol.⁷⁷ Besides, the route would be beneficial even if the “bi-functional mechanism” discussed above were to be factored in. The route may follow the synthesis protocol employed here since it directly yields Pt–Ru NPs of fcc/hcp metallic alloy type character. It may aim at Pt–Ru NPs with Pt : Ru ratio close to 50 : 50 or somewhat lower if the amount of scarce Pt in nanoalloy catalysts is to be reduced. In the latter case, the post-synthesis treatment of Pt–Ru NPs may need to be conducted so that Pt species segregate at NP surface in a way consistent with goals (i), (ii) and (iii) formulated above. Indeed adjusting parameters of a post-synthesis treatment of the type carried out here, such as duration, temperature and gas atmosphere of the treatment, is emerging as a rather fruitful procedure for optimizing the atomic structure of binary and ternary metal alloy NPs with respect to their catalytic properties.^{78,79}

Conclusions

Catalytic activity of metallic NPs is governed by a series of destruction and creation of bonds between NP surface atoms and chemical species adsorbed at NP surface. Complete or partial alloying of metal species at the nanoscale can modify the electronic structure, hence, size (or *vice versa*) and arrangement of individual metallic species at NP surface thus influencing the catalytic activity of metallic NPs significantly. The

arrangement, size, and electronic structure of atoms at NP surface, however, strongly depend on the way atoms in the layer(s) beneath it are positioned. Therefore, detailed knowledge of the atomic-scale structure across metallic alloy NPs is a prerequisite to achieving a better understanding of their catalytic properties and, hence, enabling a rational design approach to producing and optimizing metallic alloy NPs for catalytic applications.

Here we show how such knowledge can be obtained by total scattering experiments coupled to atomic PDFs analysis and 3D computer modeling. Using Pt–Ru alloy NPs as an example, we also show how, once obtained, it can be used for establishing atomic structure–catalytic properties relationships in metallic NPs. In particular, we show that electronic effects, resulting from increased interactions between Pt and Ru species near NP surface, and practically unrecognized so far atomic ensemble effects, resulting from particular configuring both of atomic layers and individual metallic species near NP surface, contribute to an increase in the catalytic activity of Pt_xRu_{100–x} alloy NPs for gas-phase oxidation of CO and electro-oxidation of ethanol at $x \sim 50$. Furthermore, keep using Pt–Ru alloy NPs as an example, we demonstrate how NP atomic structure-properties relationships can help steer synthesis and post-synthesis treatment of metallic NPs toward further improvement of their functionality. In particular, we suggest routes to improving the catalytic activity of Pt–Ru alloy NPs by enhancing the electronic and atomic ensemble effects in the NPs.

Based on results of present and prior studies^{16,39,46,47,80,81} we argue that the demonstrated here approach to establishing and making use of synthesis-atomic structure-properties relationships in metallic NPs is both widely applicable in terms of metallic NP composition and environment and easily accessible thanks to widespread instrumentation for total scattering experiments and already available computer power and relevant software. It may be added that detailed knowledge of the atomic structure across metallic NPs is very much needed when NPs are explored not only for catalytic but also magnetic and biomedical applications. For example, it can help estimate the contribution of surface atoms to the so-called surface magnetism affects⁸² and achieve a better understanding of how proteins dock to the surface of metallic NPs,⁸³ respectively. Therefore, it may be envisaged that the approach to obtaining such knowledge demonstrated here will find widespread utility in many areas of science and technology of metallic NPs.

Acknowledgements

Work on this paper was supported by DOE-BES Grant DE-SC0006877. Work at the Advanced Photon Source was supported by DOE under Contract DEAC02-06CH11357.

References

- 1 B. R. Cuenya, Synthesis and catalytic properties of metal nanoparticles: Size, shape, support, composition, and oxidation state effects, *Thin Solid Films*, 2010, **518**, 3127.

- 2 X. Liu, D. Wang and Y. Li, Synthesis and catalytic properties of bimetallic nanomaterials with various architectures, *Nano Today*, 2012, **7**, 448.
- 3 J. K. Norskov and C. H. Christensen, Toward efficient hydrogen production at surfaces, *Science*, 2006, **312**, 1322.
- 4 S. Link, Z. L. Wang and M. A. El-Sayed, Alloy Formation of Gold-Silver nanoparticles and the Dependence of the Plasmon Absorption on their composition, *J. Phys. Chem.*, 1999, **103**, 3529.
- 5 S. Link and M. A. El-Sayed, Optical Properties and ultrafast dynamics of metallic nanocrystals, *Annu. Rev. Phys. Chem.*, 2003, **54**, 331.
- 6 D. Antoniuk, M. Spasova, A. Trunova, K. Fauth, A. R. Wilhelm, J. Minar, H. Ebert, M. Farle and H. Wende, Inhomogenous alloying in FePt nanoparticles as a reason for reduced magnetic moments, *J. Phys.: Condens. Matter*, 2009, **21**, 336002.
- 7 K. Kadau, M. Gruner, P. Entel and M. Kreth, Modeling structural and magnetic phase transitions in Fe-Ni nanoparticles. Phase Transitions, *Phase Transitions*, 2003, **76**, 355.
- 8 D. Alloyeau, C. Ricolleau, C. Mottet, T. Oitkawa, C. Langlois, L. Y. Bouar, N. Braidy and A. Loiseau, Size and shape effects on the order-disorder phase transition in CoPt nanoparticles, *Nat. Mater.*, 2009, **8**, 940.
- 9 P. Tartaj, M. d. P. Morales, S. Veintemillas-Verdaguer, T. Gonzalez-Carreno and C. J. Serna, The preparation of magnetic nanoparticles for applications in biomedicine, *J. Phys. D: Appl. Phys.*, 2003, **36**, R182.
- 10 J. R. Lakowicz, Radiative decay engineering: Biophysical and biomedical applications, *Anal. Biochem.*, 2001, **298**, 1.
- 11 C.-A. J. Lin, C.-H. Lee, J.-T. Hsieh, H. H. Wang, J. K. Li, J. L. Shen, W. H. Chan, H.-I. Yeh and W. H. Chang, Synthesis of fluorescent metallic toward biomedical application: recent progress and present challenges, *Jpn. J. Med. Electron. Biol. Eng.*, 2009, **29**, 276.
- 12 J. M. Thomas and W.-J. Thomas, *Principle and practice of heterogeneous catalysis*, VCN, 1997.
- 13 W. J. Huang, R. Sun, J. Tao, L. D. Menard, R. G. Nuzzo and J. M. Zuo, Coordination-dependent surface atomic contraction in nanocrystals revealed by coherent diffraction, *Nat. Mater.*, 2008, **7**, 308.
- 14 D. Marks, Experimental studies of small particle structures, *Rep. Prog. Phys.*, 1994, **57**, 603.
- 15 A. Frenkel, Solving the 3D structure of nanoparticles, *Z. Kristallogr.*, 2007, **222**, 605.
- 16 V. Petkov, B. Prasai, Y. Ren, S. Shan, J. Luo, P. Joseph and Ch. J. Zhong, Solving the nanostructure problem: exemplified on metallic alloy nanoparticles, *Nanoscale*, 2014, **6**, 10048.
- 17 L. Zhang, J. Kim, H. M. Cheng, F. Nah, K. Dudeck, R.-S. Liu, G. A. Botton and J. Zhang, A novel CO-tolerant PtRu core-shell structured electrocatalyst with rich Ru rich in core and Pt rich in shell for hydrogen oxidation reaction and its implication in PEMFCs, *J. Power Sources*, 2011, **196**, 9117.
- 18 C.-Yu. Chen, W.-H. Lai, Ch.-Ch. Chen and S.-W. Hsu, Effects on nitrogen and CO concentrations on the performance of PEMFCs with Pt-Ru anode catalyst, *J. Power Sources*, 2013, **243**, 138.
- 19 H. Kageyama, T. Ioroi, T. Kojima, H. Senoh, N. Takeichi, K. Nomura and K. Tanimoto, XAFS Analysis of Pt and Pt-Ru Catalysts for PEFCs by *In situ* Measurements under Operating Conditions in the Fluorescence Mode, *AIP Conf. Proc.*, 2007, **882**, 645.
- 20 S. Alayoglu, A. U. Nilekar, M. Mavrikakis and B. Eichhorn, Ru-Pt core-shell nanoparticles for preferential oxidation of carbon monoxide in hydrogen, *Nat. Mater.*, 2008, **7**(4), 333.
- 21 Yu.-C. Hsieh, Yu. Zhang, D. Su, V. Volkov, R. Si, L. Wu, Y. Zhu, W. An, P. Liu, P. He, S. Ye, R. R. Adzic and J. X. Wang, Ordered bilayer ruthenium-platinum core-shell NPs as CO-tolerant fuel cell catalysts, *Nat. Commun.*, 2013, **4**, 2466.
- 22 S.-Y. Huang, S.-M. Chang, Ch.-L. Lin, Ch.-H. Chen and Ch.-T. Yeh, Promotion of the electrochemical activity of a bimetallic Pt-Ru catalyst by oxygen-induced segregation, *J. Phys. Chem. B*, 2006, **110**, 23300.
- 23 S. Stoupin, E.-H. Chung, S. Chattopadhyay, C. U. Segre and E. S. Smotkin, Pt and Ru X-ray absorption Spectroscopy of PtRu anode catalysts in operating direct methanol fuel cells, *J. Phys. Chem. B*, 2006, **110**, 9932.
- 24 R. J. K. Witshire, C. R. King, A. Rose, P. P. Wells, H. Davies, M. P. Hogarth, D. Thompsett, B. Theobald, F. W. Mosselmans, M. Roberts and A. E. Russel, Effects of composition on structure and activity of PtRu/C catalysts, *Phys. Chem. Chem. Phys.*, 2009, **11**, 2305.
- 25 E. Antolini, The problem of Ru dissolution from Pt-Ru catalysts during fuel cell operation: analysis and solutions, *J. Solid State Electrochem.*, 2011, **15**, 455.
- 26 E. Antolini, Catalysts for direct ethanol fuel cells, *J. Power Sources*, 2007, **170**, 1; C. Lamy, A. Lima, V. Leruhun, F. delime, Ch. Coutanceau and J.-M. Leger, Recent Advances in the development of direct alcohol fuel cells, *J. Power Sources*, 2002, **105**, 283.
- 27 F. H. B. Lima and E. R. Gongalez, Ethanol electro-oxidation on carbon supported Pt-Ru, Pt-Rh and Pt-Rh-Ru nanoparticles, *Electrochim. Acta*, 2008, **53**, 2963.
- 28 T. Egami and S. J. L. Billinge, *Underneath the Bragg peaks: Structural Analysis of Complex Materials*, Pergamon Press, Elsevier Ltd, New York, 2003.
- 29 V. Petkov, Nanostructure by high-energy XRD, *Mater. Today*, 2008, **11**, 28.
- 30 K. Page, T. C. Hood, T. Proffen and R. B. Neder, Building and refining complete nanoparticle structures with total scattering data, *J. Appl. Crystallogr.*, 2011, **44**, 327.
- 31 A. P. Sutton and J. Chen, Long-range Finnis-Sinclair potentials, *Philos. Mag. Lett.*, 1990, **61**, 139.
- 32 Y. Kimura, Y. Qi, T. Cagin and W. Goddard III, The Quantum Sutton-Chen Many-body Potential for Properties of fcc Metals, *MRS Symp. Ser.*, 1999, **554**, 43.
- 33 J. Yin, S. Shan, M. S. Ng, L. F. Yang, D. Mott, W. Fang, N. Kang, J. Luo and C. J. Zhong, *Langmuir*, 2013, **29**, 9249.

- 34 J. Luo, N. Kariuki, L. Han, L. Wang, C. J. Zhong and T. He, Preparation and characterization of carbon-supported PtVFe electrocatalysts, *Electrochim. Acta*, 2006, **51**, 4821.
- 35 P. Dash, T. Bond, C. Fowler, W. Hou, N. Coombs and R. W. J. Scott, Rational Design of Supported PdAu Nanoparticle Catalysts from Structured Nanoparticle Precursors, *J. Phys. Chem. C*, 2009, **113**(29), 12719.
- 36 V. Petkov, RAD, a program for analysis of X-ray diffraction data from amorphous materials for personal computers, *J. Appl. Crystallogr.*, 1989, **22**, 387.
- 37 J. Yin, S. Shan, M. S. Ng, L. F. Yang, D. Mott, W. Fang, N. Kang, J. Luo and C. J. Zhong, Catalytic and Electrocatalytic Oxidation of Ethanol over Palladium-Based Nanoalloy Catalysts, *Langmuir*, 2013, **29**, 9249.
- 38 J. M. Hutchinson, Platinum-Ruthenium Binary Alloy Phase Diagram, *Platinum Met. Rev.*, 1972, **16**, 88.
- 39 V. Petkov, N. Bedford, M. R. Knecht, M. G. Weir, R. M. Crooks, W. Tang, G. Henkelman and A. Frenkel, Periodicity and Atomic Ordering in Nanosized Particles of Crystals, *J. Phys. Chem. C*, 2008, **112**, 8907.
- 40 V. Petkov, Y. Lee, S. Sun and Y. Ren, Noncrystallographic Atomic Arrangement Driven Enhancement of the Catalytic Activity of Au Nanoparticles, *J. Phys. Chem. C*, 2012, **116**, 26668.
- 41 V. Petkov, R. Loukrakpam, L. Yang, B. N. Wanjala, J. Luo, C. J. Zhong and S. Shastri, Pt-Au alloying at the nanoscale, *Nano Lett.*, 2012, **12**, 4289.
- 42 L. Farrow, P. Juhas, J. Liu, D. Bryndin, E. Bozin, J. Bloch, T. Proffen and S. Billinge, PDFfit2 and PDFgui: computer programs for studying nanostructure in crystals, *J. Phys.: Condens. Matter*, 2007, **19**, 335219.
- 43 L. Deng, W. Hu, H. Deng and S. Xiao, Surface Segregation and Structural Features of Bimetallic Au–Pt Nanoparticles, *J. Phys. Chem. C*, 2010, **114**(25), 11026.
- 44 H. Rafii-Tabar and A. S. Sutton, Long-range Finnis-Sinclair potentials for fcc metallic alloys, *Philos. Mag. Lett.*, 1991, **63**, 217.
- 45 M. W. Finnis and J. E. Sinclair, A simple empirical N-body potential for transition metals, *Philos. Mag. A*, 1984, **50**, 45.
- 46 V. Petkov, S. Shan, P. Chupas, J. Yin, L. Yang, J. Luo and C. J. Zhong, Noble-transition metal nanoparticle breathing in a reactive gas atmosphere, *Nanoscale*, 2013, **5**, 7379.
- 47 V. Petkov, S. Shastri, S. Shan, P. Joseph, J. Luo, C. J. Zhong, T. Nakamura, Y. Herhani and S. Sato, Resolving Atomic Ordering Differences in Group 11 Nanosized Metals and Binary Alloy Catalysts by Resonant High-Energy X-ray Diffraction and Computer Simulations, *J. Phys. Chem. C*, 2013, **117**, 22131.
- 48 A. V. Ruban, H. L. Skriver and J. K. Norskov, Surface segregation energies in transition-metal alloys, *Phys. Rev. B: Condens. Matter*, 1999, **59**, 15990.
- 49 Ch. W. Hill, M. S. Nasher, A. I. Frenkel, J. R. Shapley and R. G. Nuzzo, Carbon support effect on bimetallic Pt-Ru NPs formed from molecular precursors, *Langmuir*, 1999, **15**, 690 and refs. therein.
- 50 B. Hammer and J. K. Norskov, Theoretical Surface Science and catalysis – calculations and concepts, *Adv. Catal.*, 2007, **45**, 71.
- 51 F. Marooun, F. Ozanam, O. M. Magnussen and R. J. Behm, The role of atomic assemblies in the reactivity of bimetallic electrocatalysts, *Science*, 2001, **293**, 1811.
- 52 J. K. Norskov, T. Biggaard, J. Rossmeisl and C. H. Christiansen, Towards computational design of solid catalysts, *Nat. Chem.*, 2009, **1**, 3746.
- 53 M. Watanabe and S. Motoo, Electrocatalysis by ad-atoms: Part III. Enhancement of the oxidation of carbon monoxide on platinum by ruthenium ad-atoms, *J. Electroanal. Chem. Interfacial Electrochem.*, 1975, **60**, 267.
- 54 H. A. Gaisteiger, N. Markovic, P. N. Ross and E. J. Cairns, CO Electrooxidation on Well-Characterized Pt-Ru Alloys, *J. Phys. Chem.*, 1994, **98**, 617.
- 55 J. McBreen and S. Mukerjee, In situ X-ray absorption studies of a Pt-Ru electrocatalyst, *J. Electrochem. Soc.*, 1995, **142**, 3399.
- 56 R. J. Wiltshire, C. R. King, A. Rose, P. P. Wells, H. Davies, M. P. Hogarth, D. Thomsett, B. Theobald, F. W. Mosselmans, M. Roberts and A. E. Russel, Effects of composition on structure and activity of PtRu/CC catalysts, *Phys. Chem. Chem. Phys.*, 2009, **11**, 2305.
- 57 P. Hu, D. King, M. H. Lee and M. C. Payne, Orbital mixing in CO chemisorption on transition metal surfaces, *Chem. Phys. Lett.*, 1995, **246**, 73.
- 58 Q. Ge, S. Desai, M. Neurock and K. Koourtakis, CO adsorption on the surface of Pt-Ru bulk alloy, *J. Phys. Chem.*, 2001, **105**, 9533.
- 59 K.-W. Park, J.-h. Choi, N.-K. Kwon, S.-A. Lee, Y.-E. Sung, H.-Y. Ha, S.-A. Hong, H. Kim and A. Wieckowski, Chemical and electronic effects of Ni and Pt/Ru/Ni alloy particles in methanol electrooxidation, *J. Phys. Chem. B*, 2002, **106**, 1869.
- 60 A. Schlapka, M. Liska, A. Gros, U. Kasberger and P. Jacob, Surface strain vs Substrate Interaction in Heteroepitaxial Metal Layers: Pt on Ru (0001), *Phys. Rev. Lett.*, 2003, **91**, 016101.
- 61 M. Mavrikakis, B. Hammer and J. K. Norskov, Effect of strain on the reactivity of metal surfaces, *Phys. Rev. Lett.*, 1998, **81**, 2819.
- 62 T. Bligaard and J. K. Nørskov, Ligand effects in heterogeneous catalysis and electrochemistry, *Electrochim. Acta*, 2007, **52**, 5512.
- 63 R. M. Anderson, L. Zhang, J. A. Loussaert, A. I. Frenkel, G. Henkelman and R. M. Crooks, An experimental and theoretical investigation of the inversion of Pd@Pt core@shell dendrimer encapsulated NPs, *ACS Nano*, 2013, **7**, 9345.
- 64 S. G. Kwon, G. Krylova, P. J. Phillips, R. F. Klie, S. Chattopadhyay, T. Shibata, E. E. Bunel, Y. Liu, V. B. Prakapenka, B. Lee and E. V. Shevchenko, Heterogeneous nucleation and shape transformation of multi-component metallic nanostructures, *Nat. Mater.*, 2015, **14**, 215.

- 65 A. V. Evteev, E. V. Levchenko, I. V. Belova and G. E. Murch, Formation of a surface-sandwich structure in Pd-Ni NPs by interdiffusion: atomistic modeling, *Diffus. Fundam.*, 2007, **6**, 81.
- 66 L. Pauling, *The Nature of the Chemical Bond*, Cornell University Press, Ithaca, NY, 1975.
- 67 L. Pauling, Factors Determining the Average Atomic Volumes in Intermetallic Compounds, *Proc. Natl. Acad. Sci. U. S. A.*, 1987, **84**, 4754.
- 68 T. Rajasekharam and V. Seshubai, Charge Transfer on the Metallic Atom-Pair Bond, and the Crystal Structures Adopted by Intermetallic Compounds, *Acta Crystallogr., Sect. A: Fundam. Crystallogr.*, 2012, **68**, 156.
- 69 L. Giorgi, A. Pozio, C. Bracchhini, R. Giori and S. Turtu, H₂ and H₂/CO activation mechanism on Pt/C, Ru/C and Pt-Ru/C electrocatalysts, *J. Appl. Electrochem.*, 2001, **31**, 325.
- 70 S. Stoupin, E. Chung, S. Chattopadhyay, C. U. Segre and S. S. Smotkin, Pt and Ru EXFS spectroscopy on PtRu anode catalysts in operating direct methanol fuel cell, *J. Phys. Chem.*, 2006, **110**, 9932.
- 71 A. Aduayo, G. Murrieta and R. de Coss, Elastic stability and electronic structure of fcc Ti, Zr, and Hf: a first-principles study, *Phys. Rev. B: Condens. Matter*, 2002, **65**, 092106.
- 72 M. Wasniowska, W. Wulfhekel, M. Przybylski and J. Kirschner, Submonolayer regime of Co epitaxy on Pd(111): morphology and electronic structure, *Phys. Rev. B: Condens. Matter*, 2008, **78**, 035405.
- 73 A. L. Vazquez de Parga, F. J. Garcia-Vidal and R. Miranda, Detecting electronic states at stacking faults in magnetic thin films by tunneling microscopy, *Phys. Rev. Lett.*, 2000, **85**, 4365.
- 74 J. J. Mortensen, Y. Morikawa, B. Hammer and J. K. Nørskov, Density functional theory of N₂ adsorption and dissociation on a Ru (0001) surface, *J. Catal.*, 1997, **169**, 85.
- 75 M.-S. Hyun, S.-K. Kim, B. Lee, D. Peck, Y. Shul and D. Jung, Effect of NaBH₄ concentration on the characteristics of PtRu/C catalyst for the anode of DMFC prepared by the impregnation method, *Catal. Today*, 2008, **132**(1–4), 138.
- 76 C. Bock, B. MacDougall and Y. LePage, Dependence of CH₃OH oxidation activity for a wide range of PtRu alloys: Detailed analysis and new views, *J. Electrochem. Soc.*, 2004, **151**, A1269.
- 77 E. Antolini, Effect of the structural characteristics of binary Pt-Ru and ternary Pt-Ru-M fuel cell catalysts on the activity of electro-oxidation of ethanol in acid medium, *ChemSusChem*, 2013, **6**, 966.
- 78 J. Yin, S. Shan, L. Yang, D. Mott, O. Malis, V. Petkov, F. Cai, M. S. Ng, J. Luo, B. H. Chen, M. Engelhard and C. J. Zhong, Gold-Copper Nanoparticles: Nanostructural Evolution and Bi-functional Catalytic Sites, *Chem. Mater.*, 2012, **24**, 4662.
- 79 B. N. Wanjala, B. Fang, S. Shan, V. Petkov, P. Zhu, R. Loukrakpam, Y. Chen, J. Luo, J. Yin, L. Yang, M. Shao and C. J. Zhong, Design of ternary nanoalloy catalysts: effect of nanoscale alloying and structural perfection on electrocatalytic enhancement, *Chem. Mater.*, 2012, **24**, 4283.
- 80 M. A. Newton, K. W. Chapman, D. Thompsett and P. J. Chupas, Chasing Changing nanoparticles with time resolved Pair Distribution Function method, *J. Am. Chem. Soc.*, 2012, **134**, 5036.
- 81 S. M. Oxford, P. L. Lee, P. J. Chupas, K. W. Chapman, M. C. Kung and H. H. Kung, Study of supported PdAu bimetallic nanoparticles using *in situ* X-ray tools, *J. Phys. Chem.*, 2010, **114**, 17085.
- 82 K. Sato, Magnetic nanoparticles: When atoms move around, *Nat. Mater.*, 2009, **8**, 924–925.
- 83 G. Brancolini, D. B. Kokh, L. Calzolari, R. C. Wade and S. Corni, Docking of ubiquitin to gold nanoparticles, *ACS Nano*, 2012, **6**, 9863.